Optimal Hierarchical Radio Resource Management for HetNets with Flexible Backhaul

Naeimeh Omidvar, *Student Member, IEEE,* An Liu, *Member, IEEE,* Vincent Lau, *Fellow, IEEE,* Fan Zhang, *Student Member, IEEE,* and Mohammad Reza Pakravan, *member, IEEE*

***Abstract*—Heterogeneous networks (HetNets) have been considered as a promising architecture for upcoming 5G networks due to their high energy and spectrum efficiency. However, providing backhaul connectivity for all macro and pico base stations (BSs) in HetNets constitutes a significant share of infrastructure cost. Recently, the idea of *flexible backhaul* has drown a lot of attention both from industry and academia. Under this architecture, not all the pico BSs are connected to the backhaul, resulting in a significant reduction in the infrastructure costs. In this regard, pico BSs without backhaul connectivity need to communicate with their nearby BSs in order to have indirect accessibility to the backhaul. This makes the radio resource management (RRM) in such networks more complex and challenging. In this paper, we address the problem of cross-layer RRM in HetNets with flexible backhaul. We formulate the RRM problem as a two timescale non-convex stochastic optimization problem which jointly optimizes flow control, routing control, interference mitigation and link scheduling in order to maximize a generic network utility. By exploiting the *hidden convexity* of this non-convex problem, we propose an iterative algorithm which is converges to the global optimal solution. The proposed solution has low complexity and requires low signalling and message passing among different nodes, which makes it scalable. Moreover, due to the proposed two-timescale design, it is robust to the backhaul signalling latency as well. Simulation results demonstrate the significant performance gain of the proposed solution over various baselines.**

***Index Terms*—Flexible backhaul, heterogeneous networks, cross-layer radio resource management, two timescale stochastic optimization.**

I. Introduction

Heterogeneous networks (HetNets) have attracted a lot of attention as a promising approach for improving energy efficiency while providing high capacity in future mobile access networks [**?**], [**?**]. In current HetNet design, many pico cells are deployed across the network, each with fixed high-capacity backhaul connectivity that guarantees the fulfilment of the capacity demand of each hotspot [**?**]. However, it suffers from high CAPEX and OPEX [**?**]. Because in order to guarantee the fulfilment of the capacity demands, the statically allocated resource and deployment should be highly excessive, which leads to low utilization efficiency when the traffic is low. It has been shown that due to the large number of pico BSs in future HetNet deployments, providing the fixed backhaul for all BSs will lead to significantly huge increase in the the network power consumption [**?**], [**?**].

In addition, future networks should provide better support of emergency communications as well as fast recovery, in case of unpredicted crash of access points. However, in a fixed backhaul deployment, the crash of one point needs physical replacement (e.g., using an emergency communication vehicle) which suffers from slow network recovery and low reliability.

To overcome the aforementioned problems of fixed backhaul deployment, the idea of *flexible backhaul* is proposed. The concept behind flexible backhaul is to flexibly utilize any idle network resources to maximize end-to-end experience with minimal cost. The key features of flexible backhaul technology can be identified as follows:

- **Flexible utilization of system resources:** Flexibly utilizing any system resources including wired (e.g., optical fiber, cable), or wireless (e.g., microwave, idle nodes) and hybrid resources (e.g., combined optical fiber and idle nodes), in order to increase the resource utilization efficiency.
- **Dynamic resource scheduling:** Fully exploiting the degree of freedom of network resources (in terms of time, frequency, space, power, etc.), in order to maximize the transmission capability of backhaul.
- **Dynamic network topology:** Intelligently adjusting network topology and backhaul transmission strategies, in order to match the traffic varying and meet the transmission/reliability requirements.

Considering these features, the expected benefits of flexible backhaul can be categorized in four different aspects:

1) **Cost:** Lower CAPEX and OPEX will be gained through aggregation and reusing of idle system resources. Mainly, under flexible backhaul architecture, not all of the pico BSs are connected to the backhaul, resulting in a significant reduction in the infrastructure costs.
2) **End-to-end experience:** Flexible backhaul provides better user experience through flexible resource allocation.
3) **Reliability:** Intelligent topology establishment would bring higher system reliability. For example, crash of an access point will not lead to unreachability to the backhaul, since it can dynamically reroute the traffic to other access points.
4) **Interoperability:** It also provides easier inter-radio access technology (inter-RAT) interoperability as data can be routed through different RATs under flexible backhaul.

To achieve the above benefits, a proper dynamic RRM scheme should be proposed. However, RRM for flexible backhaul is much more challenging than traditional RRM for HetNets with fixed backhaul. In HetNets with flexible backhaul, the data flows associated with a BS without backhaul connectivity may ride on the idle backhaul resources of other

BSs to reach to the backhaul network. Hence, some BSs can relay for the data flows of that BS. Accordingly, multi-hop routing will be required among different BSs. This leads to higher complexity in resource allocation as well as more complex signalling and message passing that need to be efficiently dealt with. Furthermore, relaying other BSs' data flows by a BS may increase the interference in the HetNet that should be addressed as well. Accordingly, the existing RRM schemes for HetNets with fixed backhaul cannot be applied to HetNets with flexible backhaul.

On the other hand, most existing works on RRM in HetNets, only consider short-term instantaneous CSI adaptation or long-term statistical CSI adaptation. However, in most practical cases, a mixed timescale CSI knowledge is available in the HetNet: The local instantaneous CSI knowledge is available at each BS, while the global long-term statistical CSI knowledge of the network can be available at a central network controller. Therefore, in order to fully utilize the available mixed timescale CSI knowledge, a two timescale hierarchical RRM should be considered in the HetNet.

Furthermore, the existing works on two timescale RRM for HetNets are mostly based on heuristic approaches [**?**], [**?**], i.e., the RRM solution is not derived from a single optimization problem. In [**?**] authors formulate a two-timescale hierarchical RRM problem for HetNets with enhanced inter-cell interference coordination and propose an asymptotically optimal solution for high SNRs. Yet, none of these works consider multi-hop routing which is an intrinsic characteristic of HetNets with flexible backhaul.

In this paper, we focus on the problem of dynamic resource control for heterogeneous networks with flexible backhaul. We model the problem as a two timescale stochastic optimization problem and propose a two timescale control structure where the long-term controls are adaptive to the large scale fading, and the short-term control is adaptive to the local channel state information (CSI) within a pico or macro BS. In such a hierarchical RRM design, the long-term controls can be implemented centrally on an RRM server (RRMS), and the short-term controls can be updated locally at each pico or macro BS.

In general, the problem of two timescale hierarchical RRM in HetNets with flexible backhaul is highly non-trivial and there are some challenges that need to be tackled properly.

- **Non-convexity:** The overall radio resource optimization problem is non-convex. Hence, the conventional convex optimization techniques cannot be used to solve the problem.
- **Lack of Closed-form Expectation:** The stochastic optimization problem involves expectation operation in the constraints related to the average data rate of the links, which do not have closed form expression.
- **Mixed Timescale and Combinatorial Optimization Problem:** Due to the mixed timescale RRM structure, the problem belongs to two timescale stochastic optimization problem where the optimization variables change at different timescales. Moreover, the DTX control and links scheduling control variables are combinatorial variables. Therefore, the current stochastic optimization techniques such as stochastic cutting plane cannot be applied in such problem.
- **Complex Coupling between long-term and short-term control variables:** Since the average data rate constraint of the links involve both long-term and short-term control variables, there is a strong coupling between these control variables. Therefore, the short-term and long-term control variables cannot be solved independently.

To address the above challenges, we first apply the primal-dual decomposition method to decouple the optimization problem into two subproblems, inner and outer problems.The inner problem involves data flow control and routing control, while the outer problem involves long-term interference mitigation among BSs and short-term link scheduling control. The inner problem is convex and can be solved by standard convex optimization methods. On the other hand, the outer problem is non-convex and involves combinatorial optimization. Using a hidden convexity in the outer problem, we propose an iterative algorithm to find its global optimal solution. Finally, we simulate and compare our proposed solution with various baselines to illustrate the significant performance gain of our proposed solution.

II. System Model

A. Heterogeneous Network Topology

Consider the downlink of a two-tier multi-cell heterogeneous network, as illustrated in Fig. 1. Within each cell, there are one macro BS, several pico BSs and several MUs. Moreover, there exists a radio resource management server (RRMS) in the network which coordinates the resource allocation among BSs. All the BSs are connected to and controlled by this central RRMS via a low cost signalling backhaul (e.g., X2 interface in LTE [**?**]). The gray lines between RRMS and each BS indicates the control plane, which represents the signalling interface between macro/pico BSs and RRMS.

In order to reduce the backhaul cost, only the macro BSs and a portion of the pico BSs are connected to the high speed payload backhaul. The other pico BSs do not have direct access to the backhaul and hence need to communicate with the other BSs in order to reach to the backhaul. It is assumed that the set of BSs with backhaul connection is known.

There are K data flows that are to be routed from some source BSs, which have connection to the backhaul, to some destined MUs in the network. BSs need to communicate with each other to transfer these flows from the sources to the end-users in a multi-hop mode. In this regards, some BSs need to relay the data of other source BSs in order to help their data flows reach to the associated mobile users.

The total available bandwidth is divided into M subbands which are shared by the BSs for the data transmission (BS to MU or BS to BS transmission). The HetNet topology is represented by a topology graph defined below.

Definition 1. *(HetNet Topology Graph) Define the topology graph of the HetNet as a directed graph $G = \{\mathcal{N}, \mathcal{L}\}$ where $\mathcal{N}$ is the set of all BSs and MUs and $\mathcal{L}$ is the set of all directed edges (BS-to-BS or BS-to-MU links). Each edge $l \in \mathcal{L}$ is a directed link connecting its head node to its tail node,*

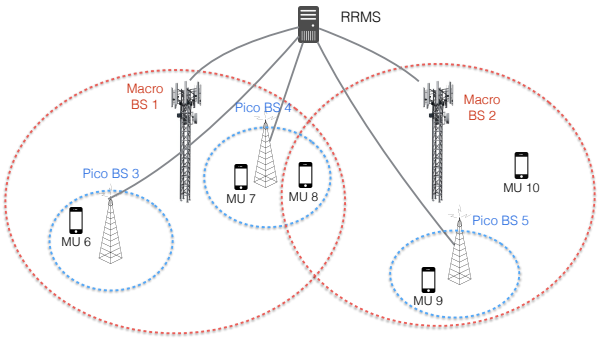

Fig. 1: A two-tier HetNet with macro and pico BSs. The signalling interface has been shown by the grey lines between RRMS and each BS. Note that the payload backhaul is not sketched in the figure for clarity.

and is associated with its CSI label $\{h_{l,m}, \forall m\}$*, where* $h_{l,m}$ *represents the channel coefficient between the head and tail nodes of the* l^{th} *link on subband* m*.*

The set of edges that are outgoing from node n is denoted by $\mathcal{T}(n)$. Note that since the coverage area of the macro BS includes the whole cell, there is direct link between the macro BS and each MU and hence, all the MUs are also associated to the macro BS as well. Moreover, let $N = |\mathcal{N}|$ and $L = |\mathcal{L}|$ be the number of nodes and links in the network topology graph.

The topology of the network can be summarized using its *node-link incidence matrix* $\boldsymbol{G}$, defined as below.

Definition 2. *(Node-link Incidence Matrix) The Node-link incidence matrix* $\boldsymbol{G}$ *for the HetNet is a* $N \times L$ *matrix, with a row for each node and a column for each link, in which its* $(n,l)^{th}$ *element is associated with node* n *and link* l *and is given by:*

$$G_{n,l} = \begin{cases} 1 & \text{if } n \text{ is the head node of link } l, \\ -1 & \text{if } n \text{ is the tail node of link } l, \\ 0 & \text{otherwise.} \end{cases} \quad (1)$$

According to the definition of the node-link incidence matrix of the network, each column corresponding to link l has one $+1$ and one -1 entries in the rows corresponding to its head and tail nodes, respectively; while all its other entries are 0. Moreover, each row of the aforementioned matrix is associated with one node in the topology graph of the network. Hence, for each BS_n, we define $\boldsymbol{g}_n$ as its associated row in the node-link incident matrix $\boldsymbol{G}$.

The corresponding topology graph for the example HetNet of Fig. 1 has been illustrated in Fig. 2. It consists of $N = 10$ nodes and $L = 17$ directed edges, representing BSs/MUs and links between them, respectively. Note that as we are considering downlink transmission, the directed links from MUs to BSs have not been included in this graph. Moreover, it can be seen from this topology graph that $\mathcal{T}(1) = \{1, 2, 4, 5, 7\}$, $\mathcal{T}(2) = \{12, 13, 14, 16\}$, $\mathcal{T}(3) = \{3, 8, 18\}$, $\mathcal{T}(4) = \{6, 9, 10, 11\}$ and $\mathcal{T}(5) = \{15, 17\}$.

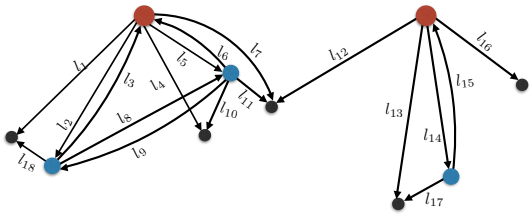

Fig. 2: The topology graph of the example HetNet of Fig. 1.

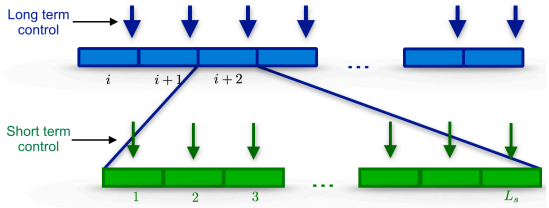

Fig. 3: Superframe and subframe structure.

Using this topology graph, it is easy to derive the node-link incidence matrix of the network, accordingly.

It can be verified that each column has exactly one 1 and one -1 elements, and its other elements are all zero. For example, consider the 5^{th} column which is associated with link 5. This column has one 1 in the first row and one -1 in the fourth row. It indicates that link 5 connects node one (which is the macro BS) to the node four (which is a pico BS) in the network.

The time domain is divided into time slots of fixed length called *superframe* as illustrated in Fig. 3. Each superframe consists of T_s *subframes*. There are M resource blocks (RBs) in each subframe t which are associated with M subbands. Each resource block is indexed by (t, m), where t determines the subframe number and m is the subband of that RB. For clarifying, we refer to superframe, subframe and RB by different indices i, t and (t, m), respectively.

As in many standard channel models, two-timescale fading model has been assumed for the wireless channels between different nodes (BS-to-BS or BS-to-MU channels). Accordingly, the channel fading coefficient is given by the following formula

$$h_{l,m}(t) = h_{l,m}^{small}(t) h_l^{large}(t), \qquad \forall l, m \quad (2)$$

where the small scale fading $H^{large} = h_{l,m}^{small}(t)$ remains constant in each subframe and changes over different subframes. On the other hand, the large scale fading process $h_l^{large}(t) > 0$ is usually caused by path loss and shadow fading, and is assumed to be a slow ergodic process, i.e., it remains constant for several superframes.

B. Two Timescale Hierarchical Radio Resource Control Variables

The radio resource management control variables are categorized into two groups called *long-term* and *short-term* control variables. The long-term control variables are determined centrally at the RRMS in the longer timescale (e.g., in each superframe) and are adaptive to the large scale fading

process $\boldsymbol{H}^{large} = \{h_l^{large},\ \forall l\}$. On the other hand, the short-term control variables are adaptive to the instantaneous CSI $\boldsymbol{H} = \{h_{l,m}^{small},\ \forall l, m\}$ and determined locally at each BS in the shorter timescale (e.g., in each subframe).

a) Long-term Control Variables

1) Flow Control: As mentioned before, there are K data flows that are to be routed in the downlink of the HetNet. We define flow control vector, $\boldsymbol{d} = [d_1, \ldots, d_K]$, in which each element d_k indicates the average allowed traffic rate for the k^{th} data flow.

As the flow control is an end-to-end control variable in the network, it should be determined centrally at the RRMS. Moreover, as they are average values, they do not need to be adapted to the short-term realizations of the channels. Hence, it is more appropriate to adapt them to the long-term statistical information of the channels, i.e., $\boldsymbol{H}^{large}$. Therefore, flow control is categorized as a long-term control variable, which is centrally determined at RRMS.

2) Routing Control: As the destined users may not be in the coverage area of their source BSs, the other BSs should help in between in order to provide an accessible routing path between the source and destination.

For generality, we assume multi-path routing is allowed in the network. It means that the traffic corresponding to each data flow k can be split arbitrarily across multiple paths between the source and destination nodes in the network. As a result, each link l may carry some part of the data flow $d_k, \forall k$. This is determined in the routing vector defined as following.

For each data flow k, the corresponding routing vector $\boldsymbol{x}_k = [x_{k,1}, \ldots, x_{k,L}]^T \in R_+^L$ is defined in which, each element $x_{k,l}$ indicates the average carried traffic of demand k over link l. Hence, the overall KL-dimensional routing vector can be defined as $\boldsymbol{x} = [\boldsymbol{x}_1^T, \ldots, \boldsymbol{x}_K^T]^T$.

The routing vectors $\{\boldsymbol{x}_k, k = 1, \ldots, K\}$ are adaptive to global network topology which is a function of the mobility of MUs and hence does not change in short timescale. Therefore these control variables are regarded as long-term control variables too and they can be determined according to statistical CSI in the longer timescale. Moreover, since they are end-to-end control variables, they are implemented centrally in RRM server.

3) Disconnected Transmission (DTX) Control: As the macro BS covers all the other nodes (i.e., all pico BSs and MUs in the cell), it can cause strong interference to them. This is called *cross-tier interference*. Moreover, pico BSs may also suffer from *co-tier interference* caused by their neighbouring pico BSs. To solve these problems, we propose *disconnected transmission* or *DTX* to eliminate the interference in the HetNet. When a DTX is scheduled in a macro or pico BS, it will shut down the transmission on the current subframe. This eliminates the interference from this BS to the other BSs. Hence, scheduling DTX over time domain allows us to control interference. Specifically, the *DTX pattern* at subframe t is denoted by $\boldsymbol{a}(t) = [a_1(t), ..., a_N(t)] \in \mathcal{A}$, where $a_n(t)$ indicates whether a DTX is scheduled for BS_n on all subbands of subframe t ($a_n(t) = 0$) or not ($a_n(t) = 1$), and $\mathcal{A}$ is the set of all interference-free (i.e., feasible) DTX patterns . Note that we may drop the index t when there is no ambiguity. In each subframe, the pattern of transmitting BSs is chosen by DTX control policy from the set of feasible DTX patterns which guarantees that no interference would be caused in the HetNet.

As the optimal DTX control policy depends on the HetNet topology graph, we control the DTX dynamically with respect to the large scale fading. Therefore, DTX control is categorized as long-term control variables.

Definition 3. *(DTX Control Policy) A DTX control policy* $\Theta = \{\boldsymbol{A}, \boldsymbol{q}\}$ *consists of a set of DTX patterns* $\boldsymbol{A} = \{\boldsymbol{a}_1, \ldots, \boldsymbol{a}_{|\boldsymbol{A}|}\}$ *with their associated time sharing* $\boldsymbol{q} = [q_1, \ldots, q_{|\boldsymbol{A}|}]^T$. *At any superframe, the DTX control policy determines that each the DTX pattern* $\boldsymbol{a}_j$ *will be used in* q_j *percentage of the subframes. The set of feasible DTX control policies is defined as*

$$\Lambda_\theta = \Big\{\Theta = \{\boldsymbol{A}, \boldsymbol{q}\}: \quad \boldsymbol{A} \subseteq \mathcal{A}, \forall i = 1, \ldots, |\boldsymbol{A}|: 0 \le q_i \le 1, \sum_{i=1}^{|\boldsymbol{A}|} q_i = 1\Big\}. \tag{3}$$

b) Short-term Control Variables

4) Dynamic Link Scheduling: As mentioned before, there are M available subbands for transmission by BSs. If the DTX pattern on the t-th subframe satisfies $\boldsymbol{a}_n(t) = 1$, BS_n is allowed to transmit on the (t, m)-th RB, $\forall m$. To avoid interference on each subband m, only one of the associated links of BS_n is scheduled for transmission on the (t, m)-th RB.

Let $\rho_{l,m} \in \{0, 1\}$ be the link scheduling variable of link l over subband m and $\boldsymbol{\rho_l} = [\rho_{l,1}, \ldots, \rho_{l,M}]^T$ be the associated subband selection vector for link l. In each subframe, this variable determines which subbands are used for transmission over link l and is decided locally by its head BS to exploit multi-user diversity as well as to avoid inter-link interference. For example, if the head BS of link l decides to use the subbands m_1 and m_2 for transmitting over link l, we would have $\rho_{l,m_1} = 1$ and $\rho_{l,m_2} = 1$.

Let $\boldsymbol{\rho} = [\boldsymbol{\rho_1}, \ldots, \boldsymbol{\rho_L}]^T$ denote the overall link scheduling vector for all the links in the network. The set of all feasible link scheduling vectors, under the DTX pattern $\boldsymbol{a}$, is given by:

$$\Lambda_\rho(\boldsymbol{a}) = \Big\{\boldsymbol{\rho} = [\boldsymbol{\rho_1}, \ldots, \boldsymbol{\rho_L}]^T: \quad \forall l: \ \boldsymbol{\rho_l} = [\rho_{l,1}, \ldots, \rho_{l,M}]^T, \quad \forall m: \ \rho_{l,m} \in \{0, 1\}, \sum_{l \in \mathcal{T}(n)} \rho_{l,m} \le a_n, \ \forall n \in \mathcal{N}\Big\}. \tag{4}$$

The intuition behind $\Lambda_{\boldsymbol{\rho}}(\boldsymbol{a})$ is elaborated below. First, each $\rho_{l,m}$ is a binary integer variable. If the m^{th} subband is used on link l, then $\rho_{l,m} = 1$. Otherwise $\rho_{l,m} = 0$ indicates that the m^{th} subband is not scheduled on link l. Moreover, if a DTX is scheduled for a BS (i.e., $a_n = 0$), none of its outgoing links can use any subband m for transmission. Finally, as both a_n and $\rho_{l,m}$ are binary, the last constraint implies that a subband can be used at most in one of the outgoing links of each BS_n.

Long-term control variables	Flow control $\boldsymbol{d}$ Routing control $\boldsymbol{x}$ DTX control Θ
Short-term control variables	Link scheduling $\boldsymbol{\rho}$

TABLE I: Summary of the long-term and short-term control variables.

This guarantees that there would be no interference among the adjacent links as well.

In each subframe, the *link scheduling policy*, selects a feasible link scheduling vector from the aforementioned feasible set, under the current DTX pattern.

Definition 4. *(Link Scheduling Policy) A link scheduling policy is a function $\boldsymbol{\rho}: \mathcal{A}\times\mathcal{H}\rightarrow\Lambda_{\boldsymbol{\rho}}(\boldsymbol{a})$, where $\mathcal{A}$ and $\mathcal{H}$ are the DTX pattern space and the CSI space, respectively. In other words, under the DTX pattern $\boldsymbol{a}$ and the channel realization $\boldsymbol{H}$, the subband(s) that are used by link l is determined by $\boldsymbol{\rho}_l=\boldsymbol{\rho}_l(\boldsymbol{a},\boldsymbol{H})=[\rho_{l,1},\ldots,\rho_{l,M}]^T,\ \forall l=1,\cdots,L$.*

For compactness, the control policies at the physical layer are summarized by a physical layer (PHY) control policy.

Definition 5. *(PHY Control Policy) We define the physical layer control policy as the combination of the DTX control policy and link scheduling control policy: $\Omega\triangleq\{\Theta,\boldsymbol{\rho}\}$, and its feasible set, Λ, is determined by:*

$$\Lambda=\left\{(\Theta,\boldsymbol{\rho})\,\middle|\,\Theta=\{\boldsymbol{A},\boldsymbol{q}\}\in\Lambda_\theta,\ \boldsymbol{\rho}\in\Lambda_{\boldsymbol{\rho}}(\boldsymbol{a}):\forall\boldsymbol{a}\in\boldsymbol{A}\right\}. \tag{5}$$

Table I summarizes the long-term and short-term control variables of our model.

III. Two Timescale Hierarchical Radio Resource Management Problem Formulation

For given DTX pattern $\boldsymbol{a}$, link scheduling policy $\boldsymbol{\rho}$ and large-scale channel fading state $\boldsymbol{H}^{large}=\{h_l^{large}\}$, the conditional average data rate carried on link l is given by:

$$r_l(\boldsymbol{a},\boldsymbol{\rho}|\boldsymbol{H}^{large})=\sum_{m=1}^{M}\mathbb{E}\left[\rho_{l,m}(\boldsymbol{a},\boldsymbol{H})\ \log(1+|h_{l,m}|^2p_l)\,\middle|\,\boldsymbol{H}^{large}\right] \tag{6}$$

where p_l is the transmission power on each subband over link l, and is given by the following equation.

$$p_l=\begin{cases}p_{macro} & \text{if the head node of link } l \text{ is a macro BS,}\\ p_{pico} & \text{if the head node of link } l \text{ is a pico BS.}\end{cases} \tag{7}$$

where p_{macro} and p_{pico} are the the power levels of macro BS and pico BS, respectively, on each subband. Since the coverage area of the macro BS is greater than the coverage area of a pico BS, it is obvious that $p_{macro}>p_{pico}$.

Note that because of the DTX pattern and link scheduling policies, there is no interference in the network.

Therefore, for a given PHY control policy $\Omega=\{\Theta,\boldsymbol{\rho}\}$, with DTX control policy $\Theta=\{\boldsymbol{A},\boldsymbol{q}\}$ and link scheduling policy $\boldsymbol{\rho}$, the average conditional data rate over link l is:

$$\overline{r}_l(\Omega|\boldsymbol{H}^{large})=\sum_{j=1}^{|\boldsymbol{A}|}q_jr_l(\boldsymbol{a}_j,\boldsymbol{\rho}|\boldsymbol{H}^{large}). \tag{8}$$

For the sake of simplicity, from now on we may use $\overline{r}_l(\Omega)$ as an abbreviated notation for $\overline{r}_l(\Omega|\boldsymbol{H}^{large})$ and define $\overline{\boldsymbol{r}}(\Omega)=[\overline{r}_1(\Omega),\ldots,\overline{r}_L(\Omega)]^T$.

The performance of the network is measured by a utility function $U(\boldsymbol{d})$, where $\boldsymbol{d}=[d_1,\ldots,d_K]$ is the average data flow vector, as mentioned before. We make the following assumption on $U(\boldsymbol{d})$.

Assumption 1. *(Utility Function) The utility function is expressed as $U(\boldsymbol{d})=\sum_{k=1}^{K}U_k(d_k)$, where U_k is a twice continuously differentiable, strictly concave and increasing function of the average data flow rate d_k, $\forall k=1,\ldots,K$.*

Note that the above assumptions on the utility function can capture a lot of interesting cases such as α-fairness and proportional fairness:

- **Alpha-fair:** This type of utility function can be used to compromise between the fairness to the users and the utilization of the resources. In this case, each function $U_k(d_k),\ \forall k$ is defined as:
$$U_k(d_k)=\begin{cases}\log(d_k+\epsilon), & \alpha=1,\\ (1-\alpha)^{-1}(d_k+\epsilon)^{1-\alpha}, & \text{Otherwise.}\end{cases} \tag{9}$$
where $\epsilon>0$ is a small number.
- **Proportional Fair (PFS):** This type of utility function is a special case of alpha-fair when $\alpha=1$ and is well-known for supporting high resource utilization while maintaining good fairness among network flows.

For a given HetNet topology graph $\mathcal{G}=\{\mathcal{N},\mathcal{L}\}$ and known source-destination pairs, the hierarchical RRM optimization problem can be formulated as following

$$\mathcal{P}_{org}:\ \max_{\boldsymbol{d},\boldsymbol{x},\Omega}\sum_{k=1}^{K}U_k(d_k) \tag{10}$$

subject to:

$$\boldsymbol{G}\boldsymbol{x}_k=\boldsymbol{v}_k(d_k),\qquad\forall k=1,\ldots,K \tag{11}$$

$$\sum_{k=1}^{K}x_{k,l}\leq\overline{r}_l(\Omega),\qquad\forall l=1,\ldots,L \tag{12}$$

$$\Omega\in\Lambda. \tag{13}$$

Constraint (11) is the flow conservation constraint, in which $\boldsymbol{G}$ is the node-link incidence matrix of the HetNet and $\boldsymbol{v}_k(d_k)\in\mathbb{R}^N$ is a vector that specifies the amount of net outgoing data rate for d_k in each node. Hence, $\boldsymbol{v}_k(d_k)=[v_{k,1},\ldots,v_{k,N}]^T$ is defined as follows:

$$v_{k,n}(d_k)=\begin{cases}d_k & \text{if } n \text{ is the source node of flow } k,\\ -d_k & \text{if } n \text{ is the destination node of flow } k,\\ 0 & \text{otherwise.}\end{cases} \tag{14}$$

Furthermore, constraint (12) is the link capacity constraint which denotes the physical layer constraint on the average data rate of each link. Finally, constraint (13) guarantees that the chosen physical layer control policy be feasible.

IV. Problem Transformation and Decomposition

According to (8), the conditional average data rate $\overline{\boldsymbol{r}} = [\overline{r}_1, \ldots, \overline{r}_L]^T$ involves stochastic expectation over CSI realizations and does not have closed-form expression. This implies that P_{org} is a stochastic optimization problem. However, since the problem includes control variables with combinatorial structure (i.e., DTX control policy), the common stochastic optimization techniques such as stochastic subgradient and stochastic cutting plane cannot be applied in this problem.

On the other hand, due to the existence of combinatorial variables (i.e., $\boldsymbol{\rho}_l, \forall l$) in the capacity constraint (12), the feasibility region of the problem is not convex. Consequently, the overall problem is not convex and hence, the conventional convex optimization techniques cannot be used to solve it.

In the following, we will show how to tackle with this challenge by transforming the original problem into a form which can exploit a hidden convexity.

Note that according to the primal decomposition [**?**], the original problem can be decomposed into two sub-problems $\mathcal{P}_1$ and $\mathcal{P}_2$, as follows.

Subproblem 1 (Optimization of the routing control $\boldsymbol{d}$ and flow control $\boldsymbol{x}$ under fixed physical layer control policy Ω):

$$\mathcal{P}_1: \ \widetilde{U}(\overline{\boldsymbol{r}}(\Omega)) = \max_{\boldsymbol{d},\boldsymbol{x}} \sum_{k=1}^{K} U_k(d_k) \tag{15}$$

s.t.:

$$\boldsymbol{G}\boldsymbol{x}_k = \boldsymbol{v}_k(d_k), \qquad \forall k = 1, \ldots, K \tag{16}$$

$$\sum_{k=1}^{K} x_{k,l} \leq \overline{r}_l(\Omega), \qquad \forall l = 1, \ldots, L. \tag{17}$$

Subproblem 2 (Optimization of physical layer control policy Ω):

$$\mathcal{P}_2: \ \max_{\Omega \in \Lambda} \widetilde{U}(\overline{\boldsymbol{r}}(\Omega)). \tag{18}$$

For any physical layer policy Ω or equivalently any data rate vector $\overline{\boldsymbol{r}}$, problem $\mathcal{P}_1$ is a standard convex optimization problem. Hence, using existing convex optimization methods, it can be easily solved in the RRMS at the beginning of each superframe in order to obtain the routing vector $\boldsymbol{x}$ and data flow rate vector $\boldsymbol{d}$ for that superframe.

Remark 1. *(Solving Problem $\mathcal{P}_1$) Note that for solving problem $\mathcal{P}_1$, we specifically use primal-dual methods. Consequently, by solving problem $\mathcal{P}_1$, we will simultaneously obtain the Lagrangian multipliers or dual variables $\boldsymbol{\lambda} = [\lambda_1, \ldots, \lambda_L]^T$ associated to constraints* (17) *as well.*

*Using the conditions in Assumption 1, [**?**, Proposition 3.3.3] shows that the Lagrangian multiplier vector $\boldsymbol{\lambda}$ is actually the gradient vector of $\widetilde{U}(\boldsymbol{r})$, i.e., $\boldsymbol{\lambda} = \nabla \widetilde{U}(\boldsymbol{r})$.*

On the other hand, it is very difficult to find the solution for problem $\mathcal{P}_2$. First, there is no closed form expression for the utility function $\widetilde{U}$ of problem $\mathcal{P}_2$ because $\widetilde{U}$ is the solution of another constrained optimization problem (i.e., problem $\mathcal{P}_1$). Moreover, the conditional average data rates $\overline{r}_l, \ \forall l$ in the objective function $\widetilde{U}(\overline{\boldsymbol{r}})$ involve stochastic expectation over CSI realizations and $\overline{r}_l$ is a non-convex function of Ω which includes combinatorial control variables $\boldsymbol{\rho}$ and $\boldsymbol{A}$. As a result, $\mathcal{P}_2$ is a non-convex stochastic optimization problem with combinatorial optimization variables and hence, the conventional stochastic optimization techniques (such as stochastic subgradient and stochastic cutting plane) cannot be applied for solving it. In the next section, we focus on addressing the following challenge.

Challenge 1. Exploit the specific structure of problem $\mathcal{P}_2$ to find a global optimal solution for this non-convex stochastic optimization problem whose objective has no closed-form expression and whose optimization variables contain combinatorial variables.

V. Solution to Problem $\mathcal{P}_2$

As elaborated before, problem $\mathcal{P}_2$ is a non-convex problem which has no closed form expression neither for the objective function or the constraints. The first challenge makes it very difficult to find a necessary and sufficient global optimality condition of this problem. In this section we aim to address the first challenge.

In this section, we first study the hidden convexity of $\mathcal{P}_2$ which can then be exploited to tackle with the first challenge and derive the global optimality condition for this problem. Next, based on the global optimality condition, we propose an iterative algorithm to efficiently solve the problem.

A. Hidden Convexity and Global Optimality Condition of $\mathcal{P}_2$

The average data rate region can be defined as:

$$\mathcal{R} = \bigcup_{\Omega \in \Lambda} \left\{ \boldsymbol{\nu} \in R_+^L : \boldsymbol{\nu} \leq \overline{\boldsymbol{r}}(\Omega) \right\}, \tag{19}$$

where $\overline{\boldsymbol{r}}(\Omega) = [\overline{r}_1(\Omega), \ldots, \overline{r}_L(\Omega)]^T$ in which $\overline{r}_l(\Omega) = \sum_{j=1}^{|\boldsymbol{A}|} q_j r_l(\boldsymbol{a_j}, \boldsymbol{\rho}), \ \forall l = 1, \ldots, L$, as earlier defined in (8).

Using this definition, Theorem 1 shows the relationship between problem $\mathcal{P}_2$ and the following optimization problem:

$$\mathcal{P}_E: \ \max_{\overline{\boldsymbol{r}} \in \mathcal{R}} \widetilde{U}(\overline{\boldsymbol{r}}). \tag{20}$$

Theorem 1. *Suppose that Ω^* is the global optimal solution of $\mathcal{P}_2$, then $\overline{\boldsymbol{r}}(\Omega^*)$ is the optimal solution of $\mathcal{P}_E$; and if $\overline{\boldsymbol{r}}^*$ is the optimal solution of $\mathcal{P}_E$, then any Ω^* satisfying $\overline{\boldsymbol{r}}(\Omega^*) = \overline{\boldsymbol{r}}^*$ is the global optimal solution of $\mathcal{P}_2$.*

Proof. Refer to Appendix A.

The following Theorem shows that the equivalent problem $\mathcal{P}_E$ is a convex problem:

Theorem 2. *(Convexity of Problem $\mathcal{P}_E$) In problem $\mathcal{P}_E$, the objective function $\widetilde{U}(\overline{\boldsymbol{r}})$ is concave and the feasible set $\mathcal{R}$ is a convex set. Hence, $\mathcal{P}_E$ is a convex optimization problem.*

Proof. The detailed proof has been provided in Appendix B.

It should be noted that although problem $\mathcal{P}_E$ is convex, it is not trivial to find its solution because its feasible set $\mathcal{R}$ still does not have any simple characterization.

The convexity of *the equivalent problem* $\mathcal{P}_E$, results in a hidden convexity in *the original problem* $\mathcal{P}_2$ which will be utilized in order to tackle with the first aforementioned challenge. For this purpose, we first express the first order optimality condition of problem $\mathcal{P}_E$ as summarized in the following lemma. Using this Lemma, Theorem 3 then derives a sufficient global optimality condition for problem $\mathcal{P}_2$.

Lemma 1. *(First Order Optimality Condition of Problem $\mathcal{P}_E$) The vector $\overline{\boldsymbol{r}}^* = [\overline{r}_1^*, \ldots, \overline{r}_L^*]^T$ is the optimal solution for problem $\mathcal{P}_E$ if*

$$\boldsymbol{g}_{\widetilde{U}}^T(\overline{\boldsymbol{r}})\Big|_{\overline{\boldsymbol{r}}=\overline{\boldsymbol{r}}^*} \cdot (\overline{\boldsymbol{r}}^* - \overline{\boldsymbol{r}}) \geq 0, \ \ \forall \overline{\boldsymbol{r}} \in \mathcal{R} \tag{21}$$

where $\boldsymbol{g}_{\widetilde{U}}(\overline{\boldsymbol{r}})$ is the gradient of $\widetilde{U}$ at point $\overline{\boldsymbol{r}}$.

Proof. Refer to Appendix C.

Using Theorem 1 and Lemma 1, Theorem 3 states a sufficient condition for global optimality for problem $\mathcal{P}_2$ as follows.

Theorem 3. *(Global Optimality Condition of $\mathcal{P}_2$) A physical layer control policy $\Omega^* = \{\Theta^*, \boldsymbol{\rho}^*\}$, where $\Theta^* = \{\boldsymbol{A}^*, \boldsymbol{q}^*\}$, is a global optimal solution of $\mathcal{P}_2$ if it satisfies the following condition:*

$$\begin{aligned} &\forall j = 1, \ldots, |\boldsymbol{A}^*|, \forall \boldsymbol{a} \in \mathcal{A}, \forall \boldsymbol{\rho} \in \Lambda_{\boldsymbol{\rho}}(\boldsymbol{a}): \\ &\boldsymbol{g}_{\widetilde{U}}^T(\overline{\boldsymbol{r}})\Big|_{\overline{\boldsymbol{r}}=\overline{\boldsymbol{r}}\left(\boldsymbol{\Omega}^*\right)} \cdot \left(\boldsymbol{r}\left(\boldsymbol{a}_j^*, \boldsymbol{\rho}^*\right) - \boldsymbol{r}(\boldsymbol{a}, \boldsymbol{\rho})\right) \geq 0 \end{aligned} \tag{22}$$

where $\boldsymbol{g}_{\widetilde{U}}(\overline{\boldsymbol{r}})\big|_{\overline{\boldsymbol{r}}=\overline{\boldsymbol{r}}(\boldsymbol{\Omega}^*)}$ is the gradient of $\widetilde{U}$ at point $\overline{\boldsymbol{r}} = \overline{\boldsymbol{r}}(\boldsymbol{\Omega}^*)$.

Proof. The detailed proof can be found in Appendix D.

B. Globally Optimal Solution of $\mathcal{P}_2$

Although Theorem 3 introduces a sufficient condition for global optimal solution of problem $\mathcal{P}_2$, achieving a solution which satisfies this condition is still non-trivial and challenging. Therefore, in order to find the optimal solution of the problem, the following challenge needs to be addressed.

Challenge 2. Find an algorithm to achieve a solution that satisfies the global optimality condition in Theorem 3.

In the rest of this section, using the global optimality condition in Theorem 3, we propose an algorithm that iteratively updates the optimization variables $\boldsymbol{A}$, $\boldsymbol{q}$, $\boldsymbol{\rho}$ and a weight vector $\boldsymbol{\omega} = [\omega_1, \ldots, \omega_L]^T$ in a way that the globally optimal solution of $\mathcal{P}_2$ is achieved. In the following, we first introduce our proposed algorithm, then we prove its properties and specifically, its global optimality.

The pseudo code of the proposed algorithm is summarized in Algorithm 1. The indexes t and i are indicators for referring to a subframe and a superframe, respectively. At each subframe $t \in [(i-1)T_s+1, iT_s]$ of the i^{th} superframe, each BS chooses a DTX pattern from the set of DTX patterns $\boldsymbol{A}^{(i)}$, based on the time-sharing vector $\boldsymbol{q}^{(i)}$ of the current superframe. It should be noted that the DTX patterns are generated at each BS using the same pseudo random generator and thus the DTX pattern generated at different BSs are the same for each subframe.

For updating the long-term control variables, at each superframe i, first, using Procedure I, a new DTX pattern $\boldsymbol{a}$ is obtained and added to the set of all previously found DTX patterns, i.e. $\boldsymbol{A}$. Then, the optimum time sharing among them is found by Procedure II. Finally, routing vector and flow control vector are updated by solving Problem $\mathcal{P}_1$, under current physical layer control policy Ω using the primal-dual method, which also finds the optimal Lagrangian multipliers $\boldsymbol{\lambda}$ of $\mathcal{P}_1$. $\boldsymbol{\lambda}$ is the gradient of the objective function $\widetilde{U}(\overline{\boldsymbol{r}})$ at $\overline{\boldsymbol{r}}(\Omega)$ and it is input to Procedure I for the next iteration. These steps are done iteratively until convergence which will be checked by the termination condition.

As mentioned above, Algorithm 1 includes two other procedures, named Procedure I and II . In the following, first we will elaborate these procedures, and then show the convergence of the the algorithm.

*1) **Procedure I (Finding a new DTX pattern $\boldsymbol{a}$)** :* For given $\boldsymbol{\omega}$, Procedure I finds a control variable $\boldsymbol{a}^*(\boldsymbol{\omega})$ that satisfies the global optimality condition in (22). Specifically, at the beginning of each superframe, RRMS broadcasts the value of $\boldsymbol{\omega}^{(i)}$ of the current superframe to all BSs. Then, using this coefficients along with local CSI, each BS_n calculates and broadcasts the average rates of each associated link conditioned on all admissible DTX patterns, based on the following equation:

$$\begin{aligned} &\forall \boldsymbol{a} \in \mathcal{A}, \forall l \in \mathcal{T}(n): \\ &r_l\left(\boldsymbol{a}, \boldsymbol{\rho}^*(\boldsymbol{a}, \boldsymbol{\omega})\right) = \sum_{m=1}^{M} \mathbb{E}\left\{\rho_{l,m}^*(\boldsymbol{a}, \boldsymbol{\omega}) \ \ \log(1 + |h_{l,m}|^2 p_l)\right\} \end{aligned} \tag{24}$$

where $\boldsymbol{\rho}^*(\boldsymbol{\omega})$ is the link scheduling policy described in (23).

Finally, at the end of each superframe, RRMS calls Procedure I to find a new DTX pattern that maximizes the overall weighted sum rate of the network based on the feedbacked conditional average rates from the BSs.

Remark 2. *The expectation term in* (24) *is over short-timescale CSI, and can be calculated by each BS knowing the distribution of short-timescale CSI. For the implementation when the distribution of the local channels are not available to BSs, this expectation term can be calculated using the running sample average over all subframes in each superframe. Moreover, the calculation of* (24) *in each BS_n does not require any message passing between BSs, and only local CSI information about the CSI of the outgoing channels from BS_n (i.e., $h_l, \ \forall l \in \mathcal{T}(n)$) is sufficient.*

*2) **Procedure II (Update of time sharing vector $\boldsymbol{q}$)** :* Having the set of chosen DTX control variables $\boldsymbol{A}^{(i)} = \left\{\boldsymbol{a}_j^{(i)}, j = 1, \cdots, |\boldsymbol{A}^{(i)}|\right\}$, along with the associated data rate of links $r_l\left(\boldsymbol{a}_j^{(i)}, \boldsymbol{\rho}^*\left(\boldsymbol{a}^{(i)}, \boldsymbol{\omega}^{(i)}\right)\right), \ \forall l$, which are feedbacked from the head BSs of the links to the RRMS, procedure II obtains the updated time sharing vector $\boldsymbol{q}^{(i)}$ by solving the following problem for fixed $\boldsymbol{A}^{(i)}$.

$$\max_{\boldsymbol{q}=[q_1,\ldots,q_{|\boldsymbol{A}^{(i)}|}]^T} \widetilde{U}(\overline{\boldsymbol{r}}) \tag{25}$$

Algorithm 1 Iterative Algorithm for Solving $\mathcal{P}_2$

1: **Initialization:**
2: Set $i = 1$, and let $\boldsymbol{A}^{(1)} = \{\boldsymbol{a}_1 \in \mathcal{A}\}$ and $\boldsymbol{q}^{(1)} = [q_1^{(1)}] = 1$.
3: Choose proper initial routing control $\boldsymbol{x}^{(1)}$ and flow control $\boldsymbol{d}^{(1)} \geq 0$ such that constraint (16) is satisfied. Let $\boldsymbol{\omega}^{(1)} = \left[\, 1 \; 1 \; \cdots \; 1 \,\right]^T$.
4: $i \leftarrow i + 1$.
5: **Step 1 (Short timescale link scheduling optimization at each BS in each subframe $t \in [(i-1)T_s + 1, iT_s]$):**
6: Each BS generates a DTX pattern $\boldsymbol{a}$ according to the current time sharing vector $\boldsymbol{q}^{(i)}$.
7: For given $\boldsymbol{\omega}^{(i)}$ of that subframe, the optimum link scheduling policy $\boldsymbol{\rho}^* \left(\boldsymbol{a}, \boldsymbol{\omega}^{(i)}\right)$ is obtained by:

$$\begin{aligned} &At\ every\ BS_n : \rho_{l_m^*,m} \leftarrow a_n^{(i)}, \\ &where\ l_m^* \triangleq \arg \max_{l \in \mathcal{T}(n)} \ \omega_l^{(i)} \log(1 + |h_{l,m}^{(i)}|^2 p_l) \end{aligned} \tag{23}$$

8: **Step 2 (Long term DTX control optimization at RRMS starting from subframe $(iT_s - T_d)$ in superframe i):**
9: **Step 2a:**
10: Call *Procedure I* with input $\boldsymbol{\omega}^{(i)}$ to obtain a new control variable $\boldsymbol{a}^*(\boldsymbol{\omega}^{(i)})$.
11: Let $\boldsymbol{A}^{(i)} = \left\{\boldsymbol{a}^*(\boldsymbol{\omega}^{(i)})\right\} \bigcup \left\{\boldsymbol{a}_j^{(i-1)} \in \boldsymbol{A}^{(i-1)} : q_j^{(i-1)} > 0\right\}$.
12: **Step 2b:**
13: Call *Procedure II* with input $\boldsymbol{A}^{(i)} = \left\{\boldsymbol{a}_1^{(i)}, \ldots, \boldsymbol{a}_{|\boldsymbol{A}^{(i)}|}^{(i)}\right\}$ to obtain the updated time sharing vector $\boldsymbol{q}^{(i)} = [q_1^{(i)}, \ldots, q_{|\boldsymbol{A}^{(i)}|}^{(i)}]^T$.
14: **Step 2c:**
15: Let $\Theta^{(i)} = \left\{\boldsymbol{A}^{(i)}, \boldsymbol{q}^{(i)}\right\}$ and $\Omega^{(i)} = \left\{\Theta^{(i)}, \boldsymbol{\rho}^{(i)}\right\}$,where the link scheduling policy $\boldsymbol{\rho}^{(i)}$ is determined by (23).
16: Solve problem $\mathcal{P}_1$ with input $\bar{\boldsymbol{r}}\left(\Omega^{(i)}\right)$, which can be calculated using the conditional average rates feedbacked from BSs to the RRMS, and obtain the updated the routing vector $\boldsymbol{x}^{(i)}$, the flow control vector $\boldsymbol{d}^{(i)}$ and the Lagrangian multipliers $\boldsymbol{\lambda}^{(i)}$.
17: Update the weight vector: $\boldsymbol{\omega}^{(i+1)} = [\omega_1^{(i+1)}, \ldots, \omega_L^{(i+1)}] = \boldsymbol{\lambda}^{(i)}$.
18: **Termination:**
19: If $\left|\widetilde{U}(\Omega^{(i)}) - \widetilde{U}(\Omega^{(i-1)})\right| \geq \epsilon$, where $\epsilon > 0$ is a small number, then the algorithm is terminated with the optimum physical layer control policy $\Omega^* = \{\Theta^*, \boldsymbol{\rho}^*\}$ where $\Theta^* = \{\boldsymbol{A}^*, \boldsymbol{q}^*\}$, $\boldsymbol{A}^* = \left\{\boldsymbol{a}_j^{(i)} : q_j^{(i)} > 0\right\}$ and $\boldsymbol{q}^* = \left[q_j^{(i)} > 0\right]$. Otherwise, return to line 4.

Algorithm 2 Procedure I: Finding a new DTX pattern $\boldsymbol{a}^*$

1: **Input** $\forall \boldsymbol{a} \in \mathcal{A} : \ r_l\left(\boldsymbol{a}, \boldsymbol{\rho}^*\left(\boldsymbol{a}, \boldsymbol{\omega}\right)\right), \ \forall l$.
2: **for** all $\boldsymbol{a} \in \mathcal{A}$ **do**
3: Let $R(\boldsymbol{a}, \boldsymbol{\omega}) = \sum_{l=1}^{L} \omega_l r_l\left(\boldsymbol{a}, \boldsymbol{\rho}^*\left(\boldsymbol{a}, \boldsymbol{\omega}\right)\right)$.
4: **end for**
5: **Output** $\boldsymbol{a}^*(\boldsymbol{\omega}) = \arg \underset{\boldsymbol{a} \in A}{max}\ R(\boldsymbol{a}, \boldsymbol{\omega})$.

subject to:

$$q_j \in [0,1], \ \forall j, \ \sum_{j=1}^{|\boldsymbol{A}^{(i)}|} q_j = 1$$

$$\overline{\boldsymbol{r}} = [\overline{r}_1, \ldots \overline{r}_L]^T, where\ \overline{r}_l = \sum_{j=1}^{|\boldsymbol{A}^{(i)}|} q_j r_l\left(\boldsymbol{a_j}^{(i)}, \boldsymbol{\rho}^*(\boldsymbol{a}^{(i)}, \boldsymbol{\omega}^{(i)})\right).$$

It can be easily verified that problem (25) is a deterministic convex optimization. Therefore, it can be efficiently solved in the RRMS using existing convex optimization methods as well.

Figure 4 illustrates the overall relationship among the main problem and the subproblems, as well as the feedback signals between BSs and the RRMS.

*3) **Optimality and Convergence of Algorithm 1**:* In this section, we show that Algorithm 1 converges to the global optimal solution of $\mathcal{P}_2$. In particular, we show that this algorithm updates the control variables in a way that the global optimality condition in Theorem 3 is satisfied. For this purpose, we first state the following Theorem about Procedure I.

Theorem 4. *(Property of Procedure I) For given input $\boldsymbol{\omega}$, the output $\boldsymbol{a}^*\left(\boldsymbol{\omega}\right)$ of Procedure I satisfies*

$$\begin{aligned} &\forall \boldsymbol{a} \in \mathcal{A}, \boldsymbol{\rho} \in \Lambda_{\boldsymbol{\rho}}\left(\boldsymbol{a}\right) : \\ &\boldsymbol{\omega}^T \cdot \left(\boldsymbol{r}\left(\boldsymbol{a}^*\left(\boldsymbol{\omega}\right), \boldsymbol{\rho}^*\left(\boldsymbol{a}^*\left(\boldsymbol{\omega}\right), \boldsymbol{\omega}\right)\right) - \boldsymbol{r}\left(\boldsymbol{a}, \boldsymbol{\rho}\right)\right) \geq 0. \end{aligned} \tag{26}$$

Proof. The detailed proof can be found in Appendix E.

Using Theorem 4, we prove the convergence of Algorithm 1 and show its maximum optimality gap in general case, via the following Theorem.

Theorem 5. *(Global Optimality of Algorithm 1) Let $\Omega^{(i)}$ be the output of the i^{th} iteration of Algorithm 1. We have*

$$\lim_{i \to \infty} \widetilde{U}\left(\Omega^{(i)}\right) = \widetilde{U}^*, \tag{27}$$

where $\widetilde{U}^*$ is the global optimal value of $\mathcal{P}_2$.

Proof. The detailed proof can be found in Appendix F.

VI. Implementation Consideration and Signalling Flow

According to our explanations for the proposed algorithm in the previous sections, the signalling flow between RRMS, macro/pico BS and MUs within each superframe or each subframe has been interpreted in Figs. 4 - 5.

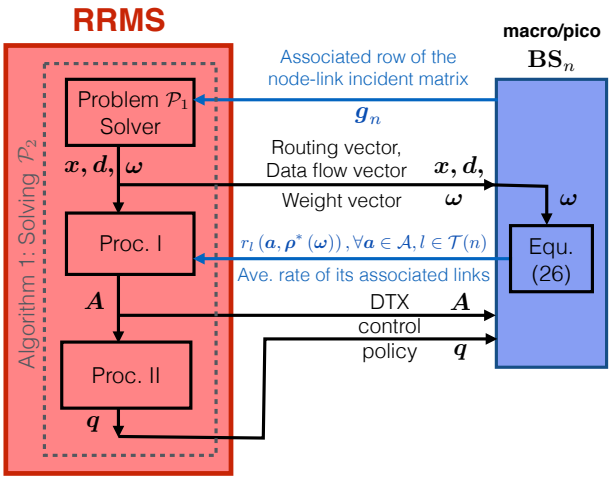

Fig. 4: Signalling flow at each superframe *(slow signalling)*.

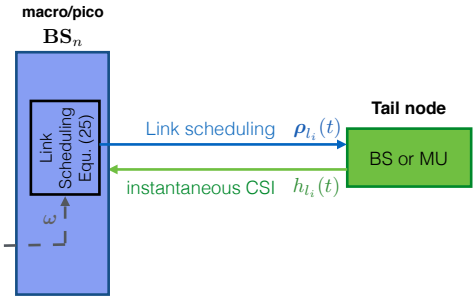

Fig. 5: Signalling flow at each subframe *(fast signalling)*.

Fig. 4 shows the *slow timescale* signalling flows that are being passed between RRMS and each BS at the end of each superframe. As can be seen in this figure, at the end of the i^{th} super frame:

1) Each BS_n sends its associated row of the node-link incident matrix (i.e., $G_{n,l}$, $\forall l$) to the RRMS so that the RRMS can have the updated information about the topology of the network. Moreover, BS_n calculates the average rates of each of its associated links conditioned on all admissible DTX patterns $r_l(\boldsymbol{a}, \boldsymbol{\rho}^*(\boldsymbol{\omega}))$, $\forall \boldsymbol{a} \in \mathcal{A}$ and send them to RRMS, for further central calculation and decision makings.
2) Then, RRMS updates the long-term control variables based on these average rates.
3) Finally, RRMS broadcasts the long-term control variables and the weight vector $\boldsymbol{\omega}$ to the BSs that will be used in the $(i+1)^{th}$ super frame.

It should be noted that we allow T_d subframes before the end of each superframe for RRMS to start to do all the above long timescale calculations and signalling. The parameter T_d is chosen as a sufficient time for calculations and message passings. This timing configuration guarantees that our design is robust to the backhaul latency.

Fig. 5 shows the *fast timescale* message passing between the head and the tail of each link, at each subframe. It is clear that the head node of each link is always a BS (macro or pico), while the tail node can be either a BS or a MU, as well.

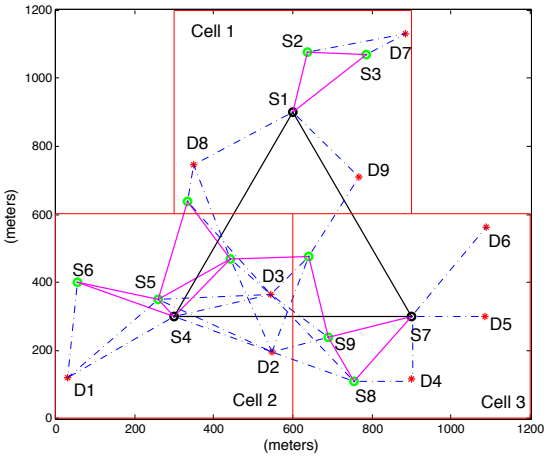

Fig. 6: Topology of a multi-cell HetNet. The source nodes and the destinations nodes has been labelled as $s_1, \cdots, s_9$ and $d_1, \cdots, d_9$, respectively. Moreover, (s_i, d_i), $\forall i = 1, \cdots, 9$, indicates each source-destination pair.

As can be comprehended from these figures, the proposed hierarchical RRM has several advantages. First, the RRMS requires only global statistical information which can be provided and feedbacked by BSs in large timescale signalling. Hence, the proposed solution is robust w.r.t. backhaul latency. On the other hand, the BSs and their associated MUs communicate locally with each other in the short timescale, while each BS only required local CSI of its outgoing direct links, which can be feedbacked by the receiving node (receiving BS or MU). Therefore, our proposed algorithm has low signalling overhead and message passing among different types of network components as well as good scalability on the complexity. Hence, it can be efficiently implemented in real applications and networks.

VII. Simulation Results

In this section, we consider a multi-cell HetNet with flexible backhaul, as shown in Fig. 6. Each red box corresponds to a macro cell. In the macro cell, there is a macro BS and 3 uniformly distributed pico BSs (constituting pico cells) and 3 active MUs. Black nodes, green nodes and small red nodes stand for macro BSs, pico BSs and MUs, respectively. Moreover, existing of a line between two nodes in this graph, shows that those nodes are in the coverage area of each other, i.e., they can communicate/interfere with each other. The solid lines show the connection links between two BSs, while the dashed lines show the links between BS and MU. The transmit power of macro BS and pico BSs are $p_{macro} = 40$ dBm and p_{pico} = 29∼35 dBm, respectively. There are 10 available subbands in the network, and 3 data flows are to be routed from cell 1/2/3 to cell 2/3/1, i.e., from some BSs connected to the backhaul to some destined users. The PFS utility (as in equation (9)) is considered.

The path-loss model for macro BS-macro BS links is based on the free space model in [**?**]. Moreover, for the pico BS-pico BS links and BS-MU links, the pass loss models of b5a scenario and c2 scenario in [**?**] have been used, respectively. For

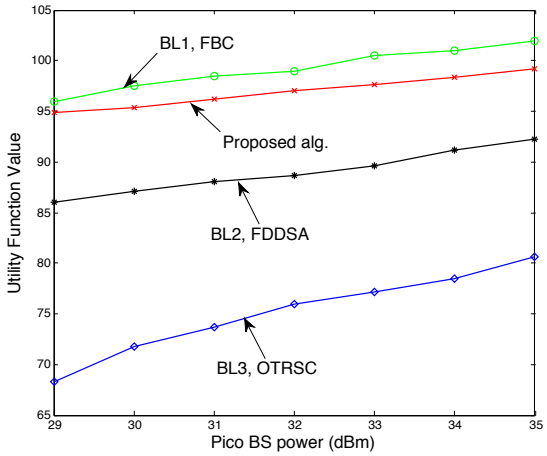

Fig. 7: Utility function comparison

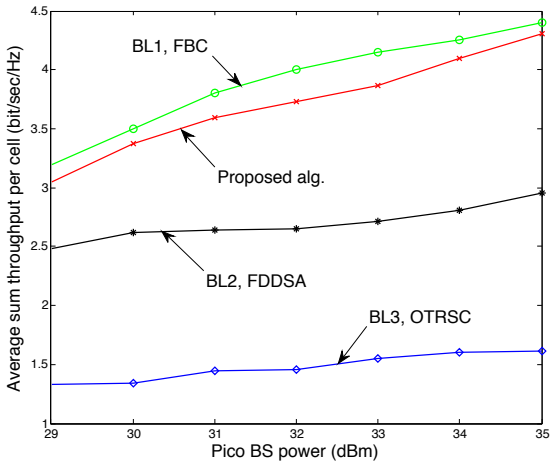

Fig. 8: Average per-cell sum throughput comparison

the small scale fading, block fading channel model has been considered, in which the small scale fading is static during one subframe and i.i.d. over different subframes. Moreover, as mentioned before, the large scale fading is considered to be a slow ergodic process which remains constant for several superframes.

A. Performance Evaluation and Comparison

We compare the performance of the proposed RRM scheme with the following baselines using numerical simulations:

- **Baseline 1, Full Backhaul Connection (FBC)**: Each pico BS is connected to the associated Macro BS in each cell. The RRM server adopted our proposed Algorithm 1 to allocate the resource.
- **Baseline 2, Fixed DTX and Dynamic Subband Allocation (FDDSA) [?]**: The RRM server selects DTX actions with equal probabilities (i.e., $q_j = \frac{1}{|\mathcal{A}|},\ \forall j = 1, \cdots, |\mathcal{A}|$) at the beginning of each frame, and the subband allocation is determined by the proposed link scheduling scheme in (23).
- **Baseline 3, One-timescale RRM adapting to Statistical CSI (TTRSC) [?]**: The RRM server solves a problem as in P_{org} with the link scheduling policy depending on the large scale fading gain instead of depending on the small scale fading gain.

Fig. 7 compares the proposed algorithm with these baselines and show the utility function versus the transmit power of pico BSs. We have also compared the performance of the proposed algorithm with the baselines in terms of the sum rate throughput, as shown in Fig. 8. As can be seen from these figure, the performance of the proposed scheme is very close to Baseline 1 (which has full backhaul connectivity) with very little performance loss due to the flexible backhaul design. Moreover, our proposed solution outperforms all the other baselines with a large gap.

B. Complexity Comparison

Table II illustrates the comparison of the MATLAB computational time of our proposed scheme and the different baselines. As it is expected, the computational time of Baseline 2 (FDDSA) is the smallest in all different scenarios, since it does not have dynamic DTX control. Moreover, the computational cost of our proposed schemes is very closes to those of Baseline 3. However, our proposed schemes outperforms baseline 1. These results verify that our proposed scheme succeeds in utilization of the local instantaneous information which is available at each BS with a low computational complexity.

No. of Cells	2	3	4
Baseline 1	13.235ms	38.201ms	80.792ms
Baseline 2	7.275ms	25.037ms	60.211ms
Baseline 3	11.189ms	36.522ms	75.314ms
Proposed Schemes	11.021ms	36.772ms	77.652ms

TABLE II: Comparison of the MATLAB computational time of the baselines and the proposed algorithm in one decision slot.

C. Convergence of the Proposed Algorithm

Fig. 9 shows the objective value $\widetilde{U}(\Omega)$ of $\mathcal{P}_2$ versus the number of iterations. As can be verified from this figure, the proposed Algorithm converges very fast.

VIII. Conclusion

In this paper, we proposed a two-timescale hierarchical RRM for HetNets with flexible backhaul. We formulate the problem with a two timescale stochastic optimization problem and considered the cross-layer design of flow control, routing control, interference mitigation and link scheduling in the heterogeneous network with flexible backhaul. Stating a sufficient condition for the optimal solution, we proposed an iterative algorithm to solve the problem. The proposed solution is optimal with low complexity. Moreover, due to the proposed two-timescale control design, it benefits from low signalling overhead and is robust to the backhaul latency as well. Simulations show that the proposed RRM design converges fast and it achieves significant performance gain over various baselines.

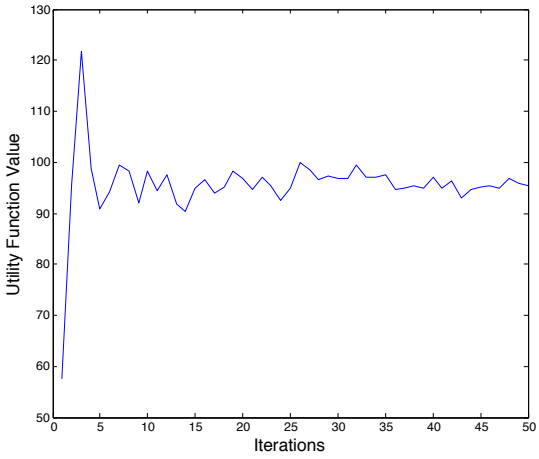

Fig. 9: Convergence result ($p_{pico} = 30$ dBm)

APPENDIX

A. Proof of Theorem 1

If Ω^* is the global optimal solution of $\mathcal{P}_2$, then from the definition of problems $\mathcal{P}_E$ and $\mathcal{P}_2$ it follows that $\overline{\boldsymbol{r}}(\Omega^*)$ would be the optimal solution of $\mathcal{P}_E$. On the other hand, suppose that $\overline{\boldsymbol{r}}^*$ is the optimal solution to $\mathcal{P}_E$, and Ω^* satisfies $\overline{\boldsymbol{r}}(\Omega^*) = \overline{\boldsymbol{r}}^*$. By contradiction, if Ω^* is not the global optimal solution of $\mathcal{P}_2$, then there exists another control policy $\Omega \in \Lambda$ such that $\widetilde{U}(\overline{\boldsymbol{r}}(\Omega)) > \widetilde{U}(\overline{\boldsymbol{r}}(\Omega^*))$. As a consequent, $\overline{\boldsymbol{r}}(\Omega^*) = \overline{\boldsymbol{r}}^*$ would not be the optimal solution of problem $\mathcal{P}_E$, and this contradicts with our first assumption.

B. Proof of Theorem 2

In order to prove the convexity of problem $\mathcal{P}_E$, we first prove that its objective function $\widetilde{U}(\overline{\boldsymbol{r}})$ is concave. Then, we prove that its feasible set is convex.

For the first part, it is sufficient to show that $-\widetilde{U}(\overline{\boldsymbol{r}})$ is convex. Note that a function is convex, if and only if its epigraph is a convex set [**?**]. The epigraph of function $-\widetilde{U}(\overline{\boldsymbol{r}})$ can be defined as $\left\{\boldsymbol{z} = \left[\begin{smallmatrix}\boldsymbol{r}\\ y\end{smallmatrix}\right] :\ \boldsymbol{r} \in \mathcal{R},\ y \geq -\widetilde{U}(\boldsymbol{r})\right\}$. Equivalently, it is sufficient to prove that the following set is convex:

$$epi\widetilde{U} \triangleq \left\{\boldsymbol{z} = \left[\begin{smallmatrix}\boldsymbol{r}\\ y\end{smallmatrix}\right] :\ \boldsymbol{r} \in \mathcal{R},\ y \leq \widetilde{U}(\boldsymbol{r})\right\}. \tag{28}$$

Lemma 2. *The set $epi\widetilde{U}$ is a convex set.*

Proof. First note that at any arbitrary $\boldsymbol{r} \in \mathcal{R}$, the Lagrangian multipliers vector $\boldsymbol{\lambda}(\boldsymbol{r})$ would be the gradient of function $\widetilde{U}$ [**?**, Proposition 3.3.3] at point $\boldsymbol{r}$. Hence, the $(L+1)$-dimensional vector $\left[\begin{smallmatrix}\boldsymbol{\lambda}(\boldsymbol{r})\\ -1\end{smallmatrix}\right]$ defines a non-vertical supporting hyperplane to $epi\widetilde{U}$ at any point $\boldsymbol{z} = \left[\begin{smallmatrix}\boldsymbol{r}\\ \widetilde{U}(\boldsymbol{r})\end{smallmatrix}\right]$, $\forall \boldsymbol{r} \in \mathcal{R}$ [**?**]; i.e.,

$$\forall \boldsymbol{r} \in \mathcal{R}: \tag{29}$$
$$(\boldsymbol{r'} - \boldsymbol{r})^T \cdot \boldsymbol{\lambda}(\boldsymbol{r}) + \left(\widetilde{U}(\boldsymbol{r}) - y'\right) \geq 0,\ \forall \boldsymbol{z'} = \left[\begin{smallmatrix}\boldsymbol{r'}\\ y'\end{smallmatrix}\right] \in epi\widetilde{U}.$$

We prove Lemma 2 by contradiction: Lets assume that $epi\widetilde{U}$ is NOT a convex set. This implies that there exists some $\boldsymbol{z_1} = \left[\begin{smallmatrix}\boldsymbol{r_1}\\ y_1\end{smallmatrix}\right], \boldsymbol{z_2} = \left[\begin{smallmatrix}\boldsymbol{r_2}\\ y_2\end{smallmatrix}\right] \in epi\widetilde{U}$ and some $0 < \alpha < 1$, such that

$$\boldsymbol{z_0} = \left[\begin{smallmatrix}\boldsymbol{r_0}\\ y_0\end{smallmatrix}\right] \triangleq \alpha \boldsymbol{z_1} + (1-\alpha)\boldsymbol{z_2} \notin epi\widetilde{U}. \tag{30}$$

According to the definition of $epi\widetilde{U}$, $\boldsymbol{r_1}$ and $\boldsymbol{r_2}$ belong to the set $\mathcal{R}$, and since it is a convex set, $\alpha \boldsymbol{r_1} + (1-\alpha)\boldsymbol{r_2} \in epi\widetilde{U}$ as well. This along with (30) implies that

$$y_0 > \widetilde{U}(\boldsymbol{r_0}). \tag{31}$$

Now consider point $\hat{\boldsymbol{z}} \triangleq \left[\begin{smallmatrix}\boldsymbol{r_0}\\ \widetilde{U}(\boldsymbol{r_0})\end{smallmatrix}\right]$. The supporting hyperplane of $epi\widetilde{U}$ at this point, so called $SHP^{epi\widetilde{U}}_{\hat{\boldsymbol{z}}}$, would be as follows.

$$SHP^{epi\widetilde{U}}_{\hat{\boldsymbol{z}}} = \Bigg\{\boldsymbol{z'} = \left[\begin{smallmatrix}\boldsymbol{r'}\\ y'\end{smallmatrix}\right] \in \mathbb{R}^{L+1}: \\ (\boldsymbol{r'} - \boldsymbol{r_0})^T \cdot \boldsymbol{\lambda}(\boldsymbol{r_0}) + \left(\widetilde{U}(\boldsymbol{r_0}) - y'\right) = 0\Bigg\}. \tag{32}$$

Substituting $\boldsymbol{r} = \boldsymbol{r_0}$ in (29), along with (31) and (32) concludes that $\boldsymbol{z_0}$ and any $\boldsymbol{z} \in epi\widetilde{U}$ are not located at the same side of the aforementioned hyperplane. In other words, we have

$$(\boldsymbol{r} - \boldsymbol{r_0})^T \cdot \boldsymbol{\lambda}(\boldsymbol{r_0}) + (y_0 - y) > 0,\ \forall \boldsymbol{z} = \left[\begin{smallmatrix}\boldsymbol{r}\\ y\end{smallmatrix}\right] \in epi\widetilde{U}. \tag{33}$$

Substituting $\boldsymbol{z} = \boldsymbol{z_1}, \boldsymbol{z_2} \in epi\widetilde{U}$ in (33) and noting that $\boldsymbol{r_0} = \alpha \boldsymbol{r_1} + (1-\alpha)\boldsymbol{r_2}$, the following two inequalities are concluded

$$(1-\alpha)(\boldsymbol{r_1} - \boldsymbol{r_2})^T \cdot \boldsymbol{\lambda}(\boldsymbol{r_0}) + (y_0 - y_1) > 0, \tag{34}$$

$$-\alpha(\boldsymbol{r_1} - \boldsymbol{r_2})^T \cdot \boldsymbol{\lambda}(\boldsymbol{r_0}) + (y_0 - y_2) > 0. \tag{35}$$

Now we multiply (34) and (35) by α and $(1-\alpha)$, respectively and then sum up the obtained inequalities together. It follows that

$$y_0 > \alpha y_1 + (1-\alpha) y_2 \tag{36}$$

where, according to (30), the right hand side expression is equal to y_0. This is obviously a contradiction and therefore Lemma 2 is proven. Consequently, the epigraph of $-\widetilde{U}$ is convex, and therefore, the objective function $\widetilde{U}(\boldsymbol{r})$ of the optimization problem $\mathcal{P}_E$ is a concave function as well. ■

Next, as in the second part of Theorem 2, we prove that the feasible set of $\mathcal{P}_E$ is convex, too.

Lemma 3. *$\mathcal{R}$ is a convex set.*

Proof. In order to prove the convexity of $\mathcal{R}$, we show that $\mathcal{R}$ is the convex hull of the following set, i.e., $\mathcal{R} = Conv(\mathcal{R}')$.

$$\mathcal{R}' = \tag{37}$$
$$\left\{\boldsymbol{r}(\boldsymbol{a}, \boldsymbol{\rho}) = [r_1(\boldsymbol{a}, \boldsymbol{\rho}), \ldots, r_L(\boldsymbol{a}, \boldsymbol{\rho})]^T : \boldsymbol{a} \in \mathcal{A}, \boldsymbol{\rho} \in \Lambda_{\boldsymbol{\rho}}(\boldsymbol{a})\right\}.$$

It is obvious that $\mathcal{R} \subset Conv(\mathcal{R}')$. Hence, it is sufficient to show that $Conv(\mathcal{R}') \subset \mathcal{R}$, too. According to the definition of $\mathcal{R}$ in (19), if any point $\boldsymbol{r}$ lies in $\mathcal{R}$, then every point $\boldsymbol{\nu} \in R^L_+$ where $\boldsymbol{\nu} \leq \boldsymbol{r}$ lies in this region as well. Therefore, in order to

prove $Conv\left(\mathcal{R}'\right) \subset \mathcal{R}$, it is sufficient to show that any Pareto boundary point $\boldsymbol{r'}$ of $Conv\left(\mathcal{R}'\right)$ lies in $\mathcal{R}$.

As $\boldsymbol{r'}$ is a L-dimensional Pareto boundary point, it can be expressed as a convex combination of $L+1$ points in $\mathcal{R}'$, i.e., $\boldsymbol{r'} = \sum_{j=1}^{L+1} q_j \boldsymbol{r}\left(\boldsymbol{a_j}, \boldsymbol{\rho}\right)$, where $\sum_{j=1}^{L+1} q_j = 1$, $q_j \in [0,1]$, $\boldsymbol{\rho} \in \Lambda_{\boldsymbol{\rho}}$ and $\boldsymbol{a_j} \in \mathcal{A}$, $\forall j$. Furthermore, as $\boldsymbol{r'}$ is a Pareto boundary point of $Conv\left(\mathcal{R}'\right)$, it follows that the point $\boldsymbol{r}\left(\boldsymbol{a_j}, \boldsymbol{\rho}\right)$, $\forall \boldsymbol{\rho}, \forall j: \ q_j > 0$ lies in the supporting hyperplane of $Conv\left(\mathcal{R}'\right)$ at the Pareto boundary point $\boldsymbol{r'}$. This fact implies that we can express $\boldsymbol{r'}$ as a convex combination of L points in the set $\left\{\boldsymbol{r}\left(\boldsymbol{a_1}, \boldsymbol{\rho}\right), \ldots, \boldsymbol{r}\left(\boldsymbol{a_{L+1}}, \boldsymbol{\rho}\right)\right\}$. Hence, $\boldsymbol{r'} = \sum_{j=1}^{L} q'_j \boldsymbol{r}\left(\boldsymbol{a'_j}, \boldsymbol{\rho}\right)$ where $\sum_{j=1}^{L} q'_j = 1$, $q'_j \in [0,1]$, $\boldsymbol{\rho} \in \Lambda_{\boldsymbol{\rho}}$ and $\boldsymbol{a'_j} \in \left\{\boldsymbol{a'_1}, \ldots, \boldsymbol{a'_L}\right\}$, $\forall j = 1, \ldots, L$. Consequently, $\boldsymbol{r'}$ lies in $\mathcal{R}$ which completes the proof of lemma 3. ■

Having Lemma 2 and Lemma 3, the proof of Theorem 2 is completed.

C. Proof of Lemma 1

Suppose $\overline{\boldsymbol{r}}^{\boldsymbol{*}} = [\overline{r}_1^*, \ldots, \overline{r}_L^*]^T$ satisfies (21) and define a function $\Psi\left(\overline{\boldsymbol{r}}\right) \triangleq \widetilde{U}\left(\overline{\boldsymbol{r}}^{\boldsymbol{*}}\right) + g_{\widetilde{U}}^T\left(\overline{\boldsymbol{r}}^{\boldsymbol{*}}\right) \cdot \left(\overline{\boldsymbol{r}} - \overline{\boldsymbol{r}}^{\boldsymbol{*}}\right)$ over the domain $\mathcal{R}$. Using the fact that $g_{\widetilde{U}}^T\left(\overline{\boldsymbol{r}}^{\boldsymbol{*}}\right)$ is the gradient of the concave function $\widetilde{U}\left(\overline{\boldsymbol{r}}\right)$ at point $\overline{\boldsymbol{r}}^{\boldsymbol{*}}$, along with the inequality in (21), it is easily to see that

$$\Psi\left(\overline{\boldsymbol{r}}\right) \geq \widetilde{U}\left(\overline{\boldsymbol{r}}\right), \ \forall \overline{\boldsymbol{r}} \in \mathcal{R}. \tag{38}$$

Moreover, we have:

$$\begin{aligned} \Psi\left(\overline{\boldsymbol{r}}^{\boldsymbol{*}}\right) &= \left.\Psi\left(\overline{\boldsymbol{r}}\right)\right|_{\overline{\boldsymbol{r}}=\overline{\boldsymbol{r}}^{\boldsymbol{*}}} = \widetilde{U}\left(\overline{\boldsymbol{r}}^{\boldsymbol{*}}\right) + g_{\widetilde{U}}^T\left(\overline{\boldsymbol{r}}^{\boldsymbol{*}}\right) \cdot \left(\overline{\boldsymbol{r}}^{\boldsymbol{*}} - \overline{\boldsymbol{r}}^{\boldsymbol{*}}\right) \\ &= \widetilde{U}\left(\overline{\boldsymbol{r}}^{\boldsymbol{*}}\right) \geq \Psi\left(\overline{\boldsymbol{r}}\right), \ \forall \overline{\boldsymbol{r}} \in \mathcal{R}. \end{aligned} \tag{39}$$

where the last inequality is clearly resulted from (21).

Combining (38) and (39), it is easily resulted that $\widetilde{U}\left(\overline{\boldsymbol{r}}^{\boldsymbol{*}}\right) \geq \widetilde{U}\left(\overline{\boldsymbol{r}}\right), \ \forall \overline{\boldsymbol{r}} \in \mathcal{R}$. Hence, $\overline{\boldsymbol{r}}^{\boldsymbol{*}}$ is the global optimal solution for problem $\mathcal{P}_E$.

D. Proof of Theorem 3

Suppose $\Omega^* = \left\{\Theta^*, \boldsymbol{\rho^*}\right\}$ with $\Theta^* = \left\{\boldsymbol{A}^*, \boldsymbol{q}^*\right\}$, $\boldsymbol{A}^* = \left\{\boldsymbol{a}_1^*, \ldots, \boldsymbol{a}_{|\boldsymbol{A}^*|}^*\right\}$ and $\boldsymbol{q}^* = \left[q_1^*, \ldots, q_{|\boldsymbol{A}^*|}^*\right]^T$ satisfies condition (22) in Theorem 3. It can be easily followed from (22) along with the definition of $\mathcal{R}$ in (19) that:

$$\left.\boldsymbol{g}_{\widetilde{U}}^T\left(\overline{\boldsymbol{r}}\right)\right|_{\overline{\boldsymbol{r}}=\overline{\boldsymbol{r}}\left(\boldsymbol{\Omega^*}\right)} \cdot \left(\boldsymbol{r}\left(\boldsymbol{a}_1^*, \boldsymbol{\rho}^*\right) - \boldsymbol{r}\right) \geq 0, \ \forall \boldsymbol{r} \in \mathcal{R}, \tag{40}$$

and

$$\begin{aligned} &\forall j = 1, \ldots, |\boldsymbol{A}^*|: \\ &\left.\boldsymbol{g}_{\widetilde{U}}^T\left(\overline{\boldsymbol{r}}\right)\right|_{\overline{\boldsymbol{r}}=\overline{\boldsymbol{r}}\left(\boldsymbol{\Omega^*}\right)} \cdot \boldsymbol{r}\left(\boldsymbol{a}_j^*, \boldsymbol{\rho}^*\right) = \left.\boldsymbol{g}_{\widetilde{U}}^T\left(\overline{\boldsymbol{r}}\right)\right|_{\overline{\boldsymbol{r}}=\overline{\boldsymbol{r}}\left(\boldsymbol{\Omega^*}\right)} \cdot \boldsymbol{r}\left(\boldsymbol{a}_1^*, \boldsymbol{\rho}^*\right). \end{aligned} \tag{41}$$

Using (41) and the fact that $\overline{r}_l\left(\Omega^*\right) = \sum_{j=1}^{|\boldsymbol{A}^*|} q_j^* r_l\left(\boldsymbol{a}_j^*, \boldsymbol{\rho}^*\right)$, and defining the l^{th} element of $\boldsymbol{g}_{\widetilde{U}}\left(\overline{\boldsymbol{r}}\right)\big|_{\overline{\boldsymbol{r}}=\overline{\boldsymbol{r}}\left(\boldsymbol{\Omega^*}\right)}$ as g_l^* for abbreviation, we will have:

$$\begin{aligned} \left.\boldsymbol{g}_{\widetilde{U}}^T\left(\overline{\boldsymbol{r}}\right)\right|_{\overline{\boldsymbol{r}}=\overline{\boldsymbol{r}}\left(\boldsymbol{\Omega^*}\right)} \cdot \overline{\boldsymbol{r}}\left(\Omega^*\right) &= \sum_{l=1}^{L} g_l^* \overline{r}_l\left(\Omega^*\right) \\ &= \sum_{j=1}^{|\boldsymbol{A}^*|} q_j^* \sum_{l=1}^{L} g_l^* r_l\left(\boldsymbol{a}_j^*, \boldsymbol{\rho}^*\right) \\ &= \sum_{j=1}^{|\boldsymbol{A}^*|} q_j^* \left.\boldsymbol{g}_{\widetilde{U}}^T\left(\overline{\boldsymbol{r}}\right)\right|_{\overline{\boldsymbol{r}}=\overline{\boldsymbol{r}}\left(\boldsymbol{\Omega^*}\right)} \cdot \boldsymbol{r}\left(\boldsymbol{a}_j^*, \boldsymbol{\rho}^*\right) \\ &= \sum_{j=1}^{|\boldsymbol{A}^*|} q_j^* \left.\boldsymbol{g}_{\widetilde{U}}^T\left(\overline{\boldsymbol{r}}\right)\right|_{\overline{\boldsymbol{r}}=\overline{\boldsymbol{r}}\left(\boldsymbol{\Omega^*}\right)} \cdot \boldsymbol{r}\left(\boldsymbol{a}_1^*, \boldsymbol{\rho}^*\right) \\ &= \left.\boldsymbol{g}_{\widetilde{U}}^T\left(\overline{\boldsymbol{r}}\right)\right|_{\overline{\boldsymbol{r}}=\overline{\boldsymbol{r}}\left(\boldsymbol{\Omega^*}\right)} \cdot \boldsymbol{r}\left(\boldsymbol{a}_1^*, \boldsymbol{\rho}^*\right) \end{aligned} \tag{42}$$

where the last equation is resulted from the fact that $\sum_{j=1}^{|\boldsymbol{A}^*|} q_j^* = 1$.

Now, combining (40) and (42), the following inequality is easily obtained.

$$\left.\boldsymbol{g}_{\widetilde{U}}^T\left(\overline{\boldsymbol{r}}\right)\right|_{\overline{\boldsymbol{r}}=\overline{\boldsymbol{r}}\left(\boldsymbol{\Omega^*}\right)} \cdot \left(\overline{\boldsymbol{r}}\left(\Omega^*\right) - \boldsymbol{r}\right) \geq 0, \ \forall \boldsymbol{r} \in \mathcal{R}. \tag{43}$$

Using Lemma 1, it follows that $\overline{\boldsymbol{r}}\left(\Omega^*\right)$ is the optimal solution of problem $\mathcal{P}_E$. Consequently, by Theorem 1, Ω^* is the global optimal solution of $\mathcal{P}_2$. This completes the proof.

E. Proof of Theorem 4

It is easy to see that for a given input $\boldsymbol{\omega}$, Procedure I outputs the optimal solution of the following optimization problem:

$$\max_{\boldsymbol{a} \in \mathcal{A}} \ \boldsymbol{\omega}^T \cdot \boldsymbol{r}\left(\boldsymbol{a}, \boldsymbol{\rho}^*\left(\boldsymbol{a}, \boldsymbol{\omega}\right)\right). \tag{44}$$

Suppose that $\boldsymbol{a}^*\left(\boldsymbol{\omega}\right)$ is the solution of the above problem. Hence, it follows that

$$\begin{aligned} &\forall \boldsymbol{a} \in \mathcal{A}, \boldsymbol{\rho} \in \Lambda_{\boldsymbol{\rho}}\left(\boldsymbol{a}\right): \\ &\boldsymbol{\omega}^T \cdot \boldsymbol{r}\left(\boldsymbol{a}^*\left(\boldsymbol{\omega}\right), \boldsymbol{\rho}^*\left(\boldsymbol{a}^*\left(\boldsymbol{\omega}\right), \boldsymbol{\omega}\right)\right) \geq \boldsymbol{\omega}^T \cdot \boldsymbol{r}\left(\boldsymbol{a}, \boldsymbol{\rho}\right), \end{aligned} \tag{45}$$

which completes the proof.

F. Proof of Theorem 5

First, we express the following Lemma which elaborates a property of Algorithm 1.

Lemma 4. *(Property of Algorithm 1) Assume that $\Omega^{(i)}$ is the physical layer control policy obtained in the i^{th} iteration of Algorithm 1 and $\boldsymbol{\omega}^{(i+1)}$ is the weight vector obtained in Step 3 of this iteration. We have*

$$\begin{aligned} \widetilde{U}\left(\Omega^{(i+1)}\right) \geq \max_{\alpha \in [0,1]} \widetilde{U}\Big(&(1-\alpha)\, \overline{\boldsymbol{r}}\left(\Omega^{(i)}\right) + \\ &\alpha\, \boldsymbol{r}\left(\boldsymbol{a}^*(\boldsymbol{\omega}^{(i+1)}), \boldsymbol{\rho}^*\left(\boldsymbol{a}^*(\boldsymbol{\omega}^{(i+1)}), \boldsymbol{\omega}^{(i+1)}\right)\right)\Big). \end{aligned} \tag{46}$$

Proof. First, according to Algorithm 1, $\widetilde{U}\left(\Omega^{(i+1)}\right)$ is the optimal value of problem (25) with $\boldsymbol{A} =$

$\left\{\boldsymbol{a}^{*}\left(\boldsymbol{\omega}^{(i+1)}\right)\right\}\bigcup\left\{\boldsymbol{a}_{j}^{(i)}\in\boldsymbol{A}^{(i)}:q_{j}^{(i)}>0\right\}$. Second, it is easy to see that $\mathbf{q}=\left[(1-\alpha)\left[\mathbf{q}^{(i)}\right]^{+};\alpha\right],\ \forall\alpha\in[0,1]$ is a feasible solution to problem (25), where $\left[\mathbf{q}^{(i)}\right]^{+}\triangleq\left\{q_{j}^{(i)}>0,\ \forall j\right\}$. Using these two facts, it is easily followed that the equation (46) holds, and hence, Lemma 4 is proved. ■

By Lemma 4, it is concluded that $\widetilde{U}\left(\Omega^{(i+1)}\right)\geq\widetilde{U}\left(\bar{\mathbf{r}}\left(\Omega^{(i)}\right)\right)=\widetilde{U}\left(\Omega^{(i)}\right)$, which implies that Algorithm 1 is increasing. This, along with the fact that the objective value is upper bounded concludes that this algorithm is convergent, i.e.,

$$\lim_{i\to\infty}\widetilde{U}\left(\Omega^{(i)}\right)=\widetilde{U}_{alg1}^{*},\tag{47}$$

where $\widetilde{U}_{alg1}^{*}$ is the convergence value of Algorithm 1.

Now, let a^{*} and Ω^{*} be any limiting points of sequences $\left\{\boldsymbol{a}^{*}\left(\boldsymbol{\omega}^{(i)}\right)\right\}$ and $\left\{\Omega^{(i)}\right\}$ generated by Algorithm 1. From (26) we have:

$$\boldsymbol{g}^{*T}\cdot\left(\boldsymbol{r}\left(a^{*}\right)-\bar{\boldsymbol{r}}^{*}\right)\geq0\tag{48}$$

where $\boldsymbol{g}^{*T}$ is the gradient of $\widetilde{U}$ at the point $\bar{\boldsymbol{r}}\left(\Omega^{*}\right)$ and $\bar{\boldsymbol{r}}^{*}$ is the global optimal solution to problem $\mathcal{P}_{2}$. Hence,

$$\begin{aligned}\widetilde{U}_{alg1}^{*}+\boldsymbol{g}^{*T}\left(\boldsymbol{r}\left(a^{*}\right)-\bar{\boldsymbol{r}}\left(\Omega^{*}\right)\right)&\geq\widetilde{U}_{alg1}^{*}+\boldsymbol{g}^{*T}\left(\bar{\boldsymbol{r}}^{*}-\bar{\boldsymbol{r}}\left(\Omega^{*}\right)\right)\\&\geq\widetilde{U}^{*}.\end{aligned}\tag{49}$$

where, the last inequality is due to the fact that $\boldsymbol{g}^{*T}$ is the gradient of the concave function $\widetilde{U}$ at the point $\bar{\boldsymbol{r}}\left(\Omega^{*}\right)$. Consequently, we have

$$\boldsymbol{g}^{*T}\cdot\left(\boldsymbol{r}\left(a^{*}\right)-\bar{\boldsymbol{r}}\left(\Omega^{*}\right)\right)\geq\widetilde{U}^{*}-\widetilde{U}_{alg1}^{*}\geq0\tag{50}$$

Now, it is sufficient to show that $\boldsymbol{g}^{*T}\cdot\left(\boldsymbol{r}\left(a^{*}\right)-\bar{\boldsymbol{r}}\left(\Omega^{*}\right)\right)=0$ which results that the convergence value of Algorithm 1 is equal to the global optimal solution of the problem, i.e., $\widetilde{U}_{alg1}^{*}=\widetilde{U}^{*}$. In the following, we will prove it by contradiction.

Assume that $\boldsymbol{g}^{*T}\cdot\left(\boldsymbol{r}\left(a^{*}\right)-\bar{\boldsymbol{r}}\left(\Omega^{*}\right)\right)>0$. Hence, from (50) it is concluded that there exist a subsequence of the iterations of Algorithm 1 such that $\boldsymbol{g}^{*T}\cdot\left(\boldsymbol{r}\left(a^{*}\right)-\bar{\boldsymbol{r}}\left(\Omega^{*}\right)\right)\geq\epsilon$, where ϵ is some positive real number. Hence, using Taylor expansion at point $\bar{\boldsymbol{r}}\left(\Omega^{*}\right)$, we have:

$$\begin{aligned}&\widetilde{U}\left(\bar{\boldsymbol{r}}\left(\Omega^{*}\right)+\tau\Big(\boldsymbol{r}\left(a^{*}\right)-\bar{\boldsymbol{r}}\left(\Omega^{*}\right)\Big)\right)=\\&\widetilde{U}\left(\bar{\boldsymbol{r}}\left(\Omega^{*}\right)\right)+\tau\boldsymbol{g}^{*T}\cdot\Big(\boldsymbol{r}\left(a^{*}\right)-\bar{\boldsymbol{r}}\left(\Omega^{*}\right)\Big)+o\left(\tau^{2}\right)\end{aligned}\tag{51}$$

for some sufficiently small $\tau>0$. This, along with the contradiction assumption, results in:

$$\widetilde{U}\left(\bar{\boldsymbol{r}}\left(\Omega^{*}\right)+\tau\Big(\boldsymbol{r}\left(a^{*}\right)-\bar{\boldsymbol{r}}\left(\Omega^{*}\right)\Big)\right)>\widetilde{U}\left(\bar{\boldsymbol{r}}\left(\Omega^{*}\right)\right)\tag{52}$$

Therefore, we have found some point $\bar{\boldsymbol{r}}\left(\Omega^{*}\right)+\tau\Big(\boldsymbol{r}\left(a^{*}\right)-\bar{\boldsymbol{r}}\left(\Omega^{*}\right)\Big)$ with strictly larger utility value than the convergence value $\widetilde{U}_{alg1}^{*}$, which contradicts with with monotonic convergence property of Algorithm 1. Accordingly, the contradiction assumption is wrong and hence, $\boldsymbol{g}^{*T}\cdot\left(\boldsymbol{r}\left(a^{*}\right)-\bar{\boldsymbol{r}}\left(\Omega^{*}\right)\right)=0$. This equation along with inequality (50) conclude that $\widetilde{U}_{alg1}^{*}=\widetilde{U}^{*}$ which completes the proof of global optimality of Algorithm 1.